View metadata, citation and similar papers at core.ac.uk

brought to you by CORE

provided by UPCommons. Portal del coneixement obert de la UPC

Properties of Cu nanoparticles-poly(N-methylpyrrole) composites

Margarita Sanchez-Jiménez,[1] Francesc Estrany[1,2,*] and Carlos Alemán,[2,3,*]

[1] *Departament d'Enginyeria Química, Escola Universitària d'Enginyeria Tècnica Industrial de Barcelona, Universitat Politècnica de Catalunya, Comte d'Urgell 187, 08036 Barcelona, Spain*

[2]*Center for Research in Nano-Engineering, Universitat Politècnica de Catalunya, Campus Sud, Edifici C', C/Pasqual i Vila s/n, Barcelona E-08028, Spain*

[3] *Departament d'Enginyeria Química, E. T. S. d'Enginyers Industrials, Universitat Politècnica de Catalunya, Diagonal 647, 08028, Barcelona, Spain*

[*] carlos.aleman@upc.edu and francesc.estrany@upc.edu

ABSTRACT

Spherical copper nanoparticles (Cu-NPs) have been immobilized on the compact surface of potentiostatically generated poly(N-methylpyrrole) (PNMPy) films by applying a reduction potential of -0.60 V to a deionized water solution of $CuCl_2$. Although the number density of Cu-NPs obtained using this procedure is not very high ($4 \cdot 10^6$ cm^{-2}), the average diameter is relatively high (~ 50 nm). The surface topology and roughness of films with Cu-NPs-PNMPy are intermediate between those obtained for as prepared PNMPy and reduced PNMPy. Analysis of the electrochemical properties indicates that Cu-NPs promote the electroactivity of the PNMPy, this effect being more evident for composited made with the thinnest PNMPy films. In opposition, the electrostability and electrical conductivity are not enhanced by deposited Cu-NPs. Similar findings are obtained for bilayered PNMPy-Cu-NPs-PNMPy films.

INTRODUCTION

The study of novel materials at the nanometric scale is one of the most challenging tasks in modern materials science, particularly with respect to nanoparticles (NPs).[1] Among various types of NPs of different sizes and compositions, metallic NPs exhibit excellent conductivity and catalytic properties, being successfully used to enhance electron transfer and catalytic processes of electrochemical reactions.[2,3] Within this field, great attention has been devoted to composite materials consisting of a mixture of metal NPs and organic polymers prepared by different methods, as for example introducing or mixing metal NPs into the organic phase. Within this context, polymer nanocomposites containing well-dipersed metallic NPs have shown to present excellent properties (*e.g.* high conductivity and stretchability),[4-11] especially when combined with conducting polymer (CPs).[6-11]

Another popular approach for the preparation of metal-NPs-CP composites consists on the chemical or physical immobilization of metallic NPs onto the surface of the CP films. Chemical immobilization is typically achieved through the formation of covalent bonds between the metal and the top of functionalized CP films,[12] whereas physical immobilization can be obtained by dropping of a colloidal solution of already synthesized NPs onto the surface[13,14] or by reducing metal ions onto the surface.[11,16,17] Among nanostructured metals, copper, with a filled 3d band, is a transition metal of fundamental interest as metallic conductor and nanomagnetic material. Indeed, Cu-NPs have been physically immobilized onto the surface of different CP films, as for example polyaniline (PAni),[18,19] poly(3-methylthiophene) (P3MT)[20] and polypyrrole (PPy).[15,17,21,22] Although the interest of some of these hybrid materials has been focused in detection applications,[18,20] in general these studies have been oriented towards the

mechanism of metallic NPs deposition rather than to improvement of CP properties.[15,19,17,21,22]

In relation with Cu-NPs-PPy composites, Cioffi *et al.*[22] deposited clusters of Cu_2O on PPy thin films from a slightly acidic (pH ~ 5) $CuCl_2$ solution. The dimensions of the clusters, which grew with the amount of Cu deposited, reached values of ~160 nm when the Cu loading was 44 mC/cm^2. Moreover, these authors found atomically dispersed Cu in the form of stabilized Cu(I)–N complexes.[22] Similar conclusions were reached by Liu *et al.*[21], who reported the interaction between the Cu atom and the pyrrolylium nitrogen through the electron transfer from the former to the latter. These authors proposed a mechanism to illustrate the metallization process by following the electrochemical deposition of Cu on PPy at a constant cathodic potential.[21] More recently, Sarkar *et al.*[17] described the growth mechanism of Cu nanocrystals on thin PPy films obtained by electropolymerization on a gold electrode. Interestingly, a variety of Cu nanostructures, including fractals, nanowires and cubic nanocrystals, was observed when Cu was electrodeposited in galvanostatic (constant current) mode while electrodeposition in potentiostatic mode (constant potential) led to a single predominant type of nanostructures. Similarly, Zhou *et al.*[15] examined the morphology and growth of uniformly sized and geometrically cubic Cu nanocrystals electrochemically deposited on PPy ultrathin films.

In this work we have examined the influence of Cu-NPs on the properties of poly(N-methylpyrrole) (PNMPy; Scheme 1), a N-methylated PPy derivative recently used for the detection of dopamine concentrations lower than that estimated for the synapse[13] and the fabrication of supercapacitors[23] and batteries[24] based on multilayered CPs. In spite of these successful applications, the electrochemical and electrical properties of PNMPy were found to be very poor,[25] which was attributed to the frequent formation of

cross-links during the polymerization process.[26] Thus, PPy forms linear chains with some irregularities in the inter-ring linkages while PNMPy tends to stabilize branched molecules with many irregularities, cross-linking being significantly higher for the latter than CP for the former one.[26] The immobilization of Cu-NPs on the surface of PNMPy films to form Cu-NPs-PNMPy composites is expected to improve the electrochemical and electric properties of the CP and, therefore, to enhance its potential use in technological applications. It should be remarked that the only antecedent combining metallic NPs and PNMPy refers to the recent study of Raso *et al.*,[27] in which PNMPy was electrochemically deposited on a previously formed layer of copper oxalates. Thus, that work, which was exclusively focused on the nucleation and growth mechanisms (*i.e.* properties of the composite were omitted), consisted on the coating of a metallic layer with the CP rather than on the coating of a CP with a metallic layer, as we propose.

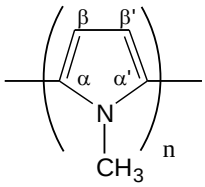

PNMPy

Scheme 1

METHODS

Materials. N-methylpyrrole (NMPy), acetonitrile, anhydrous lithium perchlorate ($LiClO_4$) and copper(II) chloride ($CuCl_2$) were purchased from Sigma-Aldrich (Spain) and used as received.

Synthesis of PNMPy. PNMPy films were prepared by chronoamperometry (CA) under a constant potential of 1.40 V[25] using a three-electrode one-compartment cell

under nitrogen atmosphere (99.995% in purity) at 25 ºC. Steel AISI 316 sheets of 4 cm^2 area were employed as working electrodes while a steel sheet of 2 cm^2 area was used as counter electrode. The reference electrode was an Ag|AgCl electrode containing a KCl saturated aqueous solution (E^o = 0.222 V *vs.* standard hydrogen electrode at 25 ºC), which was connected to the working compartment through a salt bridge containing the electrolyte solution. The cell was filled with 50 mL of 10 mM NMPy solution in acetonitrile containing 0.1 M $LiClO_4$ as supporting electrolyte. Two polymerization times, θ_P= 120 and 180 s, were considered for the different studies involved in this work. All electrochemical experiments were conducted on a PGSTAT101 AUTOLAB potenciostat-galvanostat connected to a PC computer and controlled through the NOVA 1.6 software.

Synthesis of Cu-NPs-PNMPy. Copper was deposited electrochemically onto the PNMPy films in a deionized water solution of 0.01M $CuCl_2$ and 0.1 M $LiClO_4$ under a potential of -0.60 V (versus Ag|AgCl standard potential) that was applied during a time θ_{Cu}= 60 or 120 s. Immediately after being prepared, Cu-NPs-PNMPy films were washed with distilled water and subjected to ex situ characterization. Reduced PNMPy films, hereafter denoted $PNMPy^{red}$, were prepared as blanks for comparative purposes. $PNMPy^{red}$ films were obtained by applying a reduction potential of -0.60 V during a time θ_{red}, which was identical to θ_{Cu} (θ_{red}= θ_{Cu}), to PNMPy films in a 0.1 M $LiClO_4$ deionized water solution.

Synthesis of PNMPy-Cu-NPs-PNMPy. Bilayered systems were prepared by depositing a new PNMPy layer onto the Cu-NPs-PNMPy film. This was achieved by immersing the steel electrode coated with the Cu-NPs-PNMPy composite in a 10 mM NMPy acetonitrile solution containing 0.1 M $LiClO_4$, and applying a potential of 1.40 V during θ_P= 180 s.

Thickness. The thickness was estimated from the mass of polymer deposited in the electrode (m_{pol}) with the procedure reported by Schirmeisen and Beck (*i.e.* considering the polymerization charge consumed in the generation of PNMPy films and the current productivity).[28] The volume of polymer deposited in the electrode (V_{pol}) was obtained with the values of m_{pol} and the density of each Cu-NPs-PNMPy composite, which was determined by flotation.

Scanning electron microscopy (SEM) and energy dispersive X-ray (EDX) spectroscopy. SEM and EDX spectroscopy studies were performed to examine the surface morphology and composition, respectively, of PNMPy and Cu-NPs-PNMPy. Dried samples placed in a Focussed Ion Beam Zeiss Neon 40 scanning electron microscope operating at 3 kV, equipped with an EDX spectroscopy system. Samples were mounted on a double-side adhesive carbon disc and sputter-coated with a thin layer of carbon to prevent sample charging problems.

Atomic Force Microscopy **(AFM).** Topographic AFM images were obtained with a Dimension 3100 Nanoman AFM and Multimode from Veeco using a NanoScope IV controller under ambient conditions in tapping mode. The root-mean-square roughness was determined using the statistical application of the Nanoscope software, which calculates the average considering all the values recorded in the topographic image with exception of the maximum and the minimum. AFM measurements were performed on various parts of the films, which produced reproducible images similar to those displayed in this work. The scan window size was 5×5 μm^2.

Electrochemical properties. The electrochemical properties of the studied systems were determined by CV using an acetonitrile solution with 0.1 M $LiClO_4$. The initial and final potentials were -0.5 V, and the reversal potential was 1.6 V. A scan rate of 100 $mV\cdot s^{-1}$ was used. The ability to exchange charge reversibly (*i.e.* electroactivity) and the

electrochemical stability (*i.e.* electrostability) were determined through direct measure of the anodic and cathodic areas in the control voltammograms using the GPES software. The electroactivity increases with the similarity between the anodic and cathodic areas of the first control voltammogram, whereas the electrostability decreases with the oxidation and reduction areas of consecutive control voltammograms. Specifically, the electrostability was expressed as the loss of electroactivity (LEA; in %) using the following Eqn:

$$\mathrm{LEA} = \frac{\Delta Q}{Q_{II}} \times 100 \qquad (1)$$

where ΔQ is the difference of voltammetric charges (in C) between the second and the last cycle, and Q_{II} is the voltammetric charge corresponding to the second cycle.

Electrical conductivity. The electrical conductivity was determined using the sheet resistance method with a previously described procedure.[29]

RESULTS AND DISCUSSION

The density of Cu-NPs-PNMPy composites obtained using θ_{Cu}= 60 and 120 s, which was determined by flotation using mixtures of tetrachloroethylene and carbon tetrachloride, is 1.622 and 1.639 g/cm^3, respectively. These values, which are consistent with the fact that the amount of Cu-NPs deposited on the surface of PNMPy grows with θ_{Cu}, were used to estimate the thicknesses of the films using the procedure described in the Methods section. The thickness of the Cu-NPs-PNMPy films prepared in this work, which depends on θ_P and θ_{Cu}, are: 0.84 μm for θ_P= 120 s and θ_{Cu}= 60 s; 0.99 μm for θ_P= 180 s and θ_{Cu}= 60 s; and 1.01 μm for θ_P= 120 s and θ_{Cu}= 120 s.

Figure 1 displays high and low (inset) resolution SEM micrographs of the materials prepared in this work. PNMPy films (Figure 1a) present a very compact globular

surface morphology formed by a homogeneous distribution of pseudo-spherical particles of different sizes (*i.e.* from ~100 to ~400 nm). Many of such globular particles are fused, the absence of pores providing a very dense and compact aspect. This morphology, which is independent of the polymerization time θ_P, undergoes small changes upon application of a reduction potential of -0.60 V. More specifically, the discontinuities between grouped globular particles are slightly larger in $PNMPy^{red}$ films (Figure 1b) than in PNMPy, which has been attributed to the escape of the perchlorate anions from the polymeric matrix upon reduction.

Inspection of the micrographs of Cu-NPs-PNMPy films (Figure 1c) reveals the presence of thin cracks, which are clearly oriented following a preferential direction (Figure 1c, inset). In addition of such cracks and small discontinuities between groups of globular particles, which are similar to those observed for $PNMPy^{red}$, micrographs reveal the presence of a few spherical-like particles onto the surface of the film that have attributed to potentiostatically deposited Cu-NPs. The abundance of the Cu-NPs (number density of $4 \cdot 10^6$ cm^{-2}) is significantly lower than that observed for Cu-NPs potentiostatically deposited onto PPy by applying a reduction potential of -1.20 V to a water solution of 0.05M $CuSO_4$ and 0.1 M $NaClO_4$ (number density ~$4 \cdot 10^9$ cm^{-2}).[15] However, the average diameter is significantly larger for the cupper particles produced in this work (~500 nm) than for those deposited onto the surface of PPy using the above mentioned conditions (50-100 nm). As it was expected, deposition of a PNMPy layer on the Cu-NPs-PNMPy films results in a very compact globular morphology (Figure 1d) practically identical to that obtained for PNMPy. Semi-quantitative EDX analyses were carried out for PNMPy and Cu-NPs-PNMPy films. These elemental analyses (Figure 1e) corroborated that the spherical-like particles detected at the surface of Cu-NPs-PNMPy films correspond to Cu-NPs.

The influence of Cu-NPs on surface topology and topography was examined using AFM. 2D and 3D AFM images of PNMPy, PNMPy^{red}, Cu-NPs-PNMPy and PNMPy-Cu-NPs-PNMPy films are displayed in Figure 2. PNMPy films prepared using θ_P= 180 s show multiple featured little grain boundaries with a fairly uniform surface (Figure 2a). Reduction of PNMPy to produce PNMPy^{red} provokes the apparition of relatively large surface protuberances (Figure 2b), which have been attributed to the enlargement of grain boundaries. This size increment is accompanied of a significant reduction (~50%) of the roughness. Thus, the roughness of PNMPy (Rq= 186 nm) decreases to Rq= 91 nm when the dopant ions escape from the polymeric matrix. Deposition of Cu-NPs onto PNMPy results in a topography for the CP that is intermediate between those of PNMPy and PNMPy^{red} films. Thus, Cu-NPs-PNMPy (Figure 2c) shows many polygonal grain boundaries directionally arranged in a relatively uniform surface. Similarly, the roughness of Cu-NPs-PNMPy (Rq= 155 nm) is comprised between those of oxidized and reduced PNMPy films. Finally, Figure 2d evidences that the grain boundaries observed for Cu-NPs-PNMPy are flattened in PNMPy-Cu-NPs-PNMPy because of the covering effects of the second CP layer. This feature provokes a drastic reduction of the surface roughness, which decreases to Rq= 39 nm.

Figure 3a compares the control voltammograms of PNMPy^{red} and Cu-NPs-PNMPy prepared using θ_P= 180 s and θ_{red}=θ_{Cu}= 60 s. The Cu-NPs-NMPy voltammogram shows a well-defined oxidation peak, O_1, with anodic peak potential $E_p^a(O_1)$ = 0.140 V, which has been attributed to the oxidation of metallic copper at the surface to Cu^{2+}. A second intense oxidation peak, O_2, with anodic peak potential $E_p^a(O_2)$ = 1.45 V appears overlapping another oxidation peak, O_3, whose peak potential is higher than the reverse potential. The peaks O_2 and O_3 should be interpreted as the formation of abundant

polarons and bipolarons, respectively, in the polymeric structure. The cathodic scan shows two poorly defined reduction shoulders, R_1 and R_2, with cathodic peak potentials $E_p^c(R_1)$ = 0.40 V and $E_p^c(R_2)$ = -0.20 V, which corresponds to the reduction of polarons. As the oxidized Cu^{2+} cations undergo a diffusive phenomenon away from the electrode surface, no reduction peak is expected for the $Cu^{2+} \rightarrow Cu^0$ process. These results evidence the low reduction ability of Cu-NPs-PNMPy. As it was expected, the voltammogram recorded for $PNMPy^{red}$ was very similar, with the obvious exception of O_1 that is not detected, showing also poor redox capacity. However, the oxidation peaks identified in the $PNMPy^{red}$ voltammogram are not only less pronounced but also lower in terms of anodic intensity than the oxidation peaks found for Cu-NPs-PNMPy, which clearly indicates that Cu-NPs enhances the electroactive response of PNMPy at the anodic scan.

The effect of the thickness in the electrochemical characteristics of $PNMPy^{red}$ and Cu-NPs-PNMPy films is displayed in Figure 3b, which represent the control voltammograms of films prepared using θ_P= 120 s and $\theta_{red}=\theta_{Cu}$= 60 s. The most remarkable difference with respect to the voltammograms displayed in Figure 3a refers to the reduction process R_2 (with $E_p^c(R_2)$ = -0.35 and -0.14 V for $PNMPy^{red}$ and Cu-NPs-PNMPy, respectively), which is better defined and more intense than those found in the voltammograms of films prepared using θ_P= 180 s. This feature clearly indicates that the redox capability of $PNMPy^{red}$ and Cu-NPs-PNMPy films improves with decreasing thickness, which has been attributed to the fact that undesirable cross-linking increases with the polymerization time.[26] Thus, the mobility of dopant ions at the interface polymer-electrolyte solution upon oxidation and reduction processes is higher for films generated using θ_P= 120 s than for those using θ_P= 180 s. Furthermore, it is

worth noting that cathodic and anodic areas are higher for Cu-NPs-PNMPy voltammograms than for PNMPy^{red} ones (Figures 3a and 3b), evidencing that Cu-NPs promotes the electroactivity of PNMPy, independently of θ_P.

The voltammogram of the Cu-NPs-PNMPy sample prepared using θ_P= 120 s and θ_{Cu}= 120 s, which is displayed in Figure 3c, shows a loss of definition in the anodic scan as compared with that displayed in Figure 3b while the reduction peaks in the cathodic are more clearly defined, especially R_2 with $E_p^c(R_2)$ = -0.27 V. In contrast the voltammogram obtained for the PNMPy^{red} film prepared using these conditions is very similar to that displayed in Figure 3b, indicating that the reduction time has a negligible effect in absence of $CuCl_2$. The overall of the results displayed in Figure 3 allow us to conclude that, as expected, the electroactivity of PNMPy films increases upon deposition of Cu-NPs and, in addition, the redox capability of Cu-NPs-PNMPy films increases by decreasing θ_P. However, the cathodic is the only electrochemical response of Cu-NPs-PNMPy that is improved by increasing θ_{Cu}.

The variation of the electroactivity with the number of consecutive oxidation-reduction cycles (Eqn 1) is represented in Figure 4a, measured voltammetric charge being displayed in Figure 4b. For films prepared using identical polymerization conditions, the loss of electroactivity is in all cases higher for Cu-NPs-PNMPy than for PNMPy^{red}. Furthermore, it is worth noting that the electrostability of Cu-NPs-PNMPy films is independent of θ_P, whereas electrochemical stability clearly grows with θ_{Cu}= 120 s. For example, after 15 cycles the loss of electroactivity of the films prepared using θ_{Cu}= 60 and 120 s (both with θ_P= 180 s) is 61% and 44%, respectively. These results are consistent with the enhancement of the cathodic response that, as showed above (Figure 3), increases with θ_{Cu}. The overall of the results displayed in Figure 4 allow us to

conclude that the deposition of Cu-NPs does not provide any benefit in terms of electrochemical stability. On the other hand, systematic EDX analyses (not shown) revealed that the amount of Cu-NPs decreases progressively with increasing number of redox cycles. In spite of this, compositions obtained by EDX clearly showed that Cu-NPs are still present on the surface of all samples after 16 cycles.

In recent studies we found that multilayered films prepared using a multiple polymerization steps strategy show better electrochemical properties than films made using a single polymerization step.[30-32] This improvement is due to the synergistic effect produced by favorable interactions at the interfaces. Within this context, properties of bilayered PNMPy-Cu-NPs-PNMPy and PNMPy-PNMPy^{red} are compared in Figure 5. Voltamograms displayed in Figure 5a reflect that the electroactivity of PNMPy-Cu-NPs-PNMPy is significantly higher (~300%) than that of PNMPy-PNMPy^{red}. Thus, the favorable impact of Cu-NPs in the capability of PNMPy to exchange charge reversibly is magnified in bilayered systems, indicating that Cu-NPs enhance the above mentioned synergistic effect. However, the electrochemical stability of PNMPy-Cu-NPs-PNMPy films is, unfortunately, lower than those determined for PNMPy-PNMPy^{red} (Figures 5b and 5c), this behavior being similar to that observed for monolayered systems (Figure 4).

The electrical conductivities (κ) measured at room temperature for PNMPy-Cu-NPs-PNMPy and PNMPy-PNMPy^{red} films are $\kappa = 3.8 \cdot 10^{-3}$ and $4.2 \cdot 10^{-3}$ S/cm, these values being practically identical to that obtained for PNMPy films prepared using θ_P= 360 s (*i.e.* $\kappa = 5.2 \cdot 10^{-3}$ S/cm). This observation is qualitatively similar to that found for PPy films with Cu-NPs deposited onto the surface.[33] More specifically, the incorporation of Cu-NPs onto PPy films does not promote en increment of the electrical conductivity, even though PPy is reported to e more conducting than PNMPy.[33] After 24h the

electrical conductivity of these PNMPy-Cu-NPs-PNMPy, PNMPy-PNMPy^{red} and PNMPy films decreased to $\kappa = 9.3 \cdot 10^{-4}$, $2.1 \cdot 10^{-3}$ and $3.3 \cdot 10^{-3}$ S/cm, respectively, and after 48 h $\kappa = 8.0 \cdot 10^{-4}$, $1.9 \cdot 10^{-3}$ and $2.8 \cdot 10^{-3}$ S/cm, respectively. These results indicate that Cu-NPs do not affect the electrical conductivity of the CP. However, these NPs slightly accelerate the electrical degradation of the material, which is consistent with the electrostability results discussed above.

CONCLUSIONS

Spherical Cu-NPs have been deposited onto the surface of PNMPy films by applying a reduction potential of -0.60 V to a deionized water solution of $CuCl_2$ and $LiClO_4$. Apparently, deposition of Cu-NPs did not provoke significant changes on the surface compactness and morphology of PNMPy. SEM micrographs have indicated that the number density and diameter of Cu-NPs obtained through the experimental conditions used in this work are lower and higher, respectively, than those immobilized on PPy using a reduction potential of -1.20 V. On the other hand, the surface topography and roughness of Cu-NPs-PNMPy films are intermediate between those obtained for as prepared PNMPy and PNMPy^{red}. Thus, although the reduction potential applied for the deposition of Cu-NPs enlarges the grain boundaries of PNMPy, this increment is significantly smaller than that observed for PNMPy^{red}. Analysis of the electrochemical properties indicates that Cu-NPs promote the electroactivity of PNMPy, this effect increasing with decreasing thickness of the CP film. Interestingly, θ_{Cu} does not affect to the anodic response of the composites but only to the cathodic one, which increases with θ_{Cu}. The latter behavior is fully consistent with the variation of the electrochemical stability in Cu-NPs-PNMPy composites, which increases with θ_{Cu}. On the other hand,

the influence of Cu-NPs on the electrical conductivity is practically null, values obtained for Cu-NPs-PNMPy and PNMPy^{red} being practically identical.

ACKNOWLEDGEMENTS

This work has been supported by MICINN and FEDER funds (project number MAT2012-34498) and by the DIUE of the Generalitat de Catalunya (contracts number 2009SGR925 and XRQTC). Support for the research of C.A. was received through the prize "ICREA Academia" for excellence in research funded by the Generalitat de Catalunya.

REFERENCES

1. F. W. Campbell, and R. G. Compton, *Anal. Bioanal. Chem.*, **396**, 241 (2010).
2. L. Rassaei, M. Amiri, C.M. Cirtiu, M. Sillanpaa, F. Marken, and M. Sillanpaa, *Trends Anal. Chem.*, **30**, 1704 (2011).
3. Z. He, D. Liu, R. Li, Z. Zhou, and P. Wang, *Anal. Chim. Acta*, **747**, 29 (2012).
4. Y. Kim, J. Zhu, B. Yeom, M. Di Prima, X. Su, J.-G. Kim, S. J. Yoo, C. Uher, and N. A. Kotov, *Nature*, **500**, 59 (2013).
5. S. Vaddiraju, K. Seneca, and K. K. Gleason, *Adv. Funct. Mater.*, **18**, 1929 (2008).
6. R. Gangopadhyay, and A. De, *Chem. Mater.*, **12**, 608 (2000).
7. M. A. Breimer, G. Yevgeny, S. Sy, and O. A. Sadik, *Nano Lett.*, **1**, 305 (2001).
8. D. C. Schnitzler, M. S. Meruvia, I. A. Hümmelgen, and A. J. Zarbin, *Chem. Mater.*, **15**, 4658 (2003).
9. M.-C. Christine, and D. Astruc, *Chem. Rev.*, **104**, 293 (2004).
10. L. Zhai, and R. D. McCullough, *J. Mater. Chem.*, **14**, 141 (2004).

11. A. P. O'Mullane, S. E. Dale, J. V. Macpherson, and P. R. Unwin, *Chem. Commun.*, **14**, 1606 (2004).
12. S. Vaddiraju, K. Seneca, and K. K. Gleason, *Adv. Funct. Mater.*, **18**, 1929 (2008).
13. M. Martí, G. Fabregat, F. Estrany, C. Alemán, and E. Armelin, *J. Mater. Chem.*, **20**, 10652 (2010).
14. G. Fabregat, E. Córdova-Mateo, E. Armelin, O. Bertran, and C. Alemán, *J. Phys. Chem. C*, **115**, 14933 (2011).
15. Zhou, X. J., A. J. Harmer, N. F. Heining, and K. T. Leung, *Langmuir*, **20**, 5109 (2004).
16. H.-H. Shih, D. Williams, N. H. Mack, and H.-L. Wang, *Macromolecules*, **42**, 14 (2009).
17. D. K. Sarkar, X. J. Zhou, A. Tannous, and K. T. Leung, *J. Phys. Chem. B*, **107**, 2879 (2003).
18. Y. Zhang, J. Yin, K. Wang, P. Chen, and L. Ji, *J. Appl. Polym. Sci.*, **128**, 2971 (2013).
19. V. Tsakova, D. Borissov, B. Ranguelov, Ch. Stromberg, and J. W. Schultze, *Electrochim. Acta*, **46**, 4213 (2001).
20. C. Malitesta, M. R. Guascito, E. Mazzotta, T. Siciliano, and A. Tepore, *Sens. Actuators B*, **184**, 70 (2013).
21. Y.-C. Liu, K.-H. Yang, and M.-D. Ger, *Synth. Met.*, **126**, 337 (2002).
22. N. Cioffi, L. Torsi, I. Losito, C. Di Franco, I. De Bari, L. Chiavarone, G. Scamarcio, V. Tsakova, L. Sabbatini and P. G. Zambonin, *J. Mater. Chem.*, **11**, 1434 (2001).
23. D. Aradilla, F. Estrany, and C. Alemán, *J. Phys. Chem. C*, **115**, 8430 (2011).

24. D. Aradilla, F. Estrany, F. Casellas, J. I. Iribarren, and C. Alemán, *Org. Electr.*, **15**, 40 (2014).
25. R. Oliver, A. Muñoz, C. Ocampo, C. Alemán, and F. Estrany, *Chem. Phys.*, **328**, 299 (2006).
26. C. Alemán, J. Casanovas, O. Torras, O. Bertrán, E. Armelin, R. Oliver, and F. Estrany, *Polym.*, **49**, 1066 (2008).
27. M. A. Raso, M. J. González-Tejera, I. Carrillo, E. Sanchez de la Blanca, M. V. García, and M. I. Redondo, *Thin Solid Films*, **519**, 2387 (2011).
28. M. Schirmeisen, and F.J. Beck, *J. Appl. Electrochem.*, **19**, 401 (1989).
29. J. Carrasco, E. Brillas, V. Fernández, P. L. Cabot, J. A. Garrido, F. Centellas, and R. M. Rodríguez, *J. Electrochem. Soc.*, **148**, E19 (2001).
30. D. Aradilla, F. Estrany, and C. Alemán, *J. Phys. Chem. C*, **115**, 8430 (2011).
31. F. Estrany, D. Aradilla, R. Oliver, E. Armelin, and C. Alemán, *Eur. Polym. J.* **44**, 1323 (2008).
32. D. Aradilla, F. Estrany, and C. Alemán, *J. Appl. Polym. Sci.*, **121**, 1982 (2011).
33. T. F. Otero, S. O. Costa, M. J. Ariza, and M. Marquez, *J. Mater. Chem.*, **15**, 1662 (2005).

CAPTIONS TO FIGURES

Figure 1. High and low (inset) resolution SEM micrographs of: (a) PNMPy (θ_P= 180 s); (b) PNMPy^{red} (θ_P= 180 s and θ_{red}= 60 s); (c) Cu-NPs-PNMPy (θ_P= 180 s and θ_{Cu}= 60 s); and (d) PNMPy-Cu-NPs-PNMPy (θ_P= 180 s and θ_{Cu}= 60 s) films. (e) EDX analysis of PNMPy (red line) and Cu-NPs-PNMPy (yellow surface).

Figure 2. 2D and 3D (left and right, respectively) AFM images of (a) PNMPy PNMPy (θ_P= 180 s), (b) PNMPy^{red} (θ_P= 180 s and θ_{red}= 60 s), (c) Cu-NPs-PNMPy (θ_P= 180 s and θ_{Cu}= 60 s) and (d) PNMPy-Cu-NPs-PNMPy (θ_P= 180 s and θ_{Cu}= 60 s) films.

Figure 3. Cyclic voltammograms of Cu-NPs-PNMPy (black) and PNMPy^{red} (grey) films prepared using: (a) θ_P= 180 s and θ_{Cu}=θ_{red}= 60 s; (b) θ_P= 120 s and θ_{Cu}=θ_{red}= 60 s; and (c) θ_P= 120 s and θ_{Cu}=θ_{red}= 120 s. Voltammograms were recorded in acetonitrile solution with 0.1 M $LiClO_4$ using a scan rate of 100 $mV \cdot s^{-1}$.

Figure 4. Variation of (a) the loss of electroactivity (LEA, in %) and (b) the measured voltammetric charge (Q, in mC/cm^2) against the number of consecutive oxidation-reduction cycles for Cu-NPs-PNMPy and PNMPy^{red} films prepared by using different polymerization (θ_P), deposition (θ_{Cu}) and reduction (θ_{red}) times.

Figure 5. (a) Cyclic voltammograms and variation of (b) the loss of electroactivity (LEA, in %) and (c) the measured voltammetric charge (Q, in mC/cm^2) against the number of consecutive oxidation-reduction cycles for PNMPy-Cu-NPs-PNMPy (black) and PNMPy-PNMPy^{red} (grey) bilayered films. Voltammograms were recorded in acetonitrile solution with 0.1 M $LiClO_4$ using a scan rate of 50 $mV \cdot s^{-1}$.

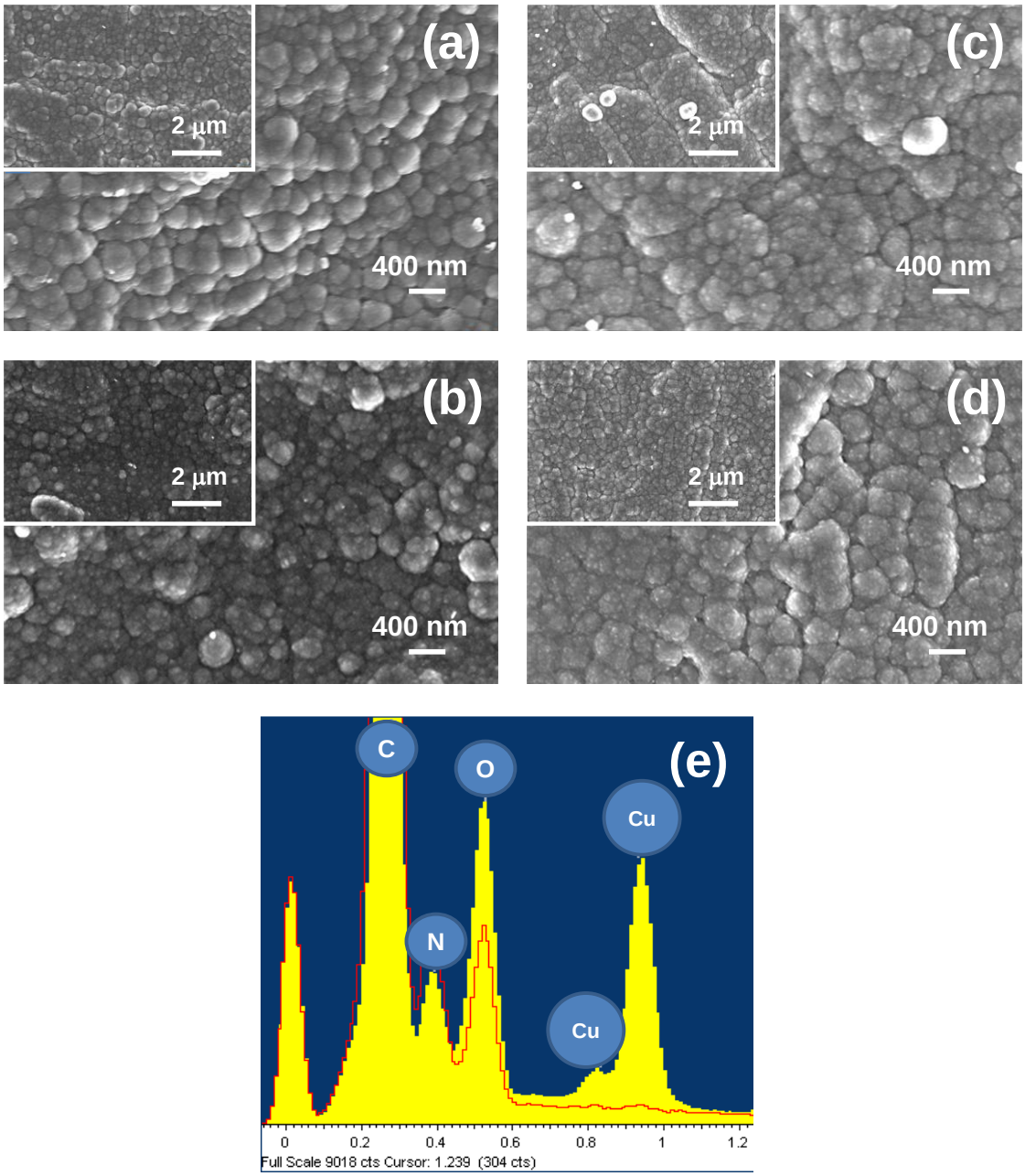
(a)
2 µm
400 nm
(c)
2 µm
400 nm
(b)
2 µm
400 nm
(d)
2 µm
400 nm
(e)
C
O
N
Cu
Cu
0
0.2
0.4
0.6
0.8
1
1.2
Full Scale 9018 cts Cursor: 1.239 (304 cts)

Figure 1

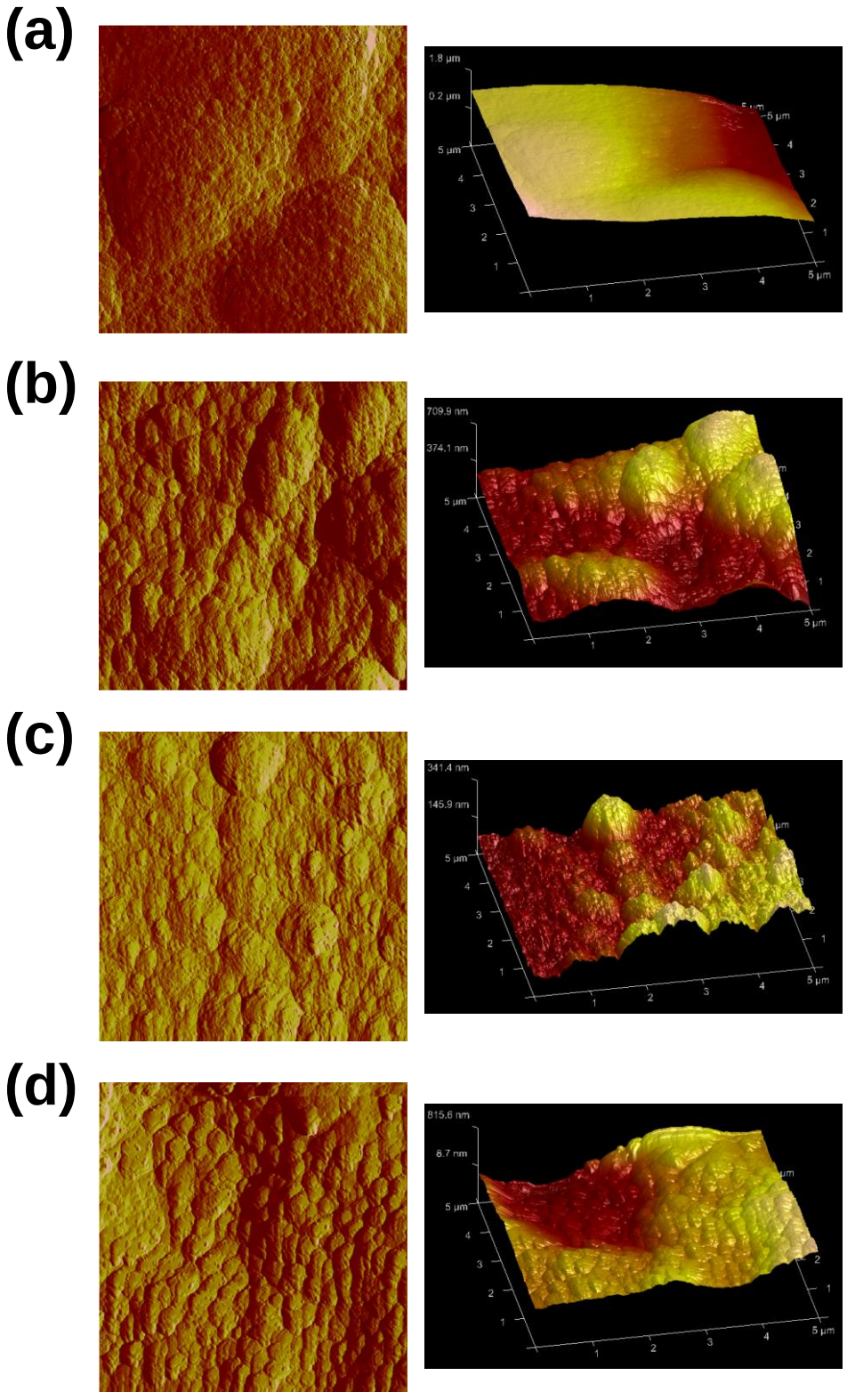
(a)
1.8 µm
0.2 µm
5 µm
5 µm
(b)
709.9 nm
374.1 nm
5 µm
5 µm
(c)
341.4 nm
145.9 nm
5 µm
5 µm
(d)
815.6 nm
8.7 nm
5 µm
5 µm

Figure 2

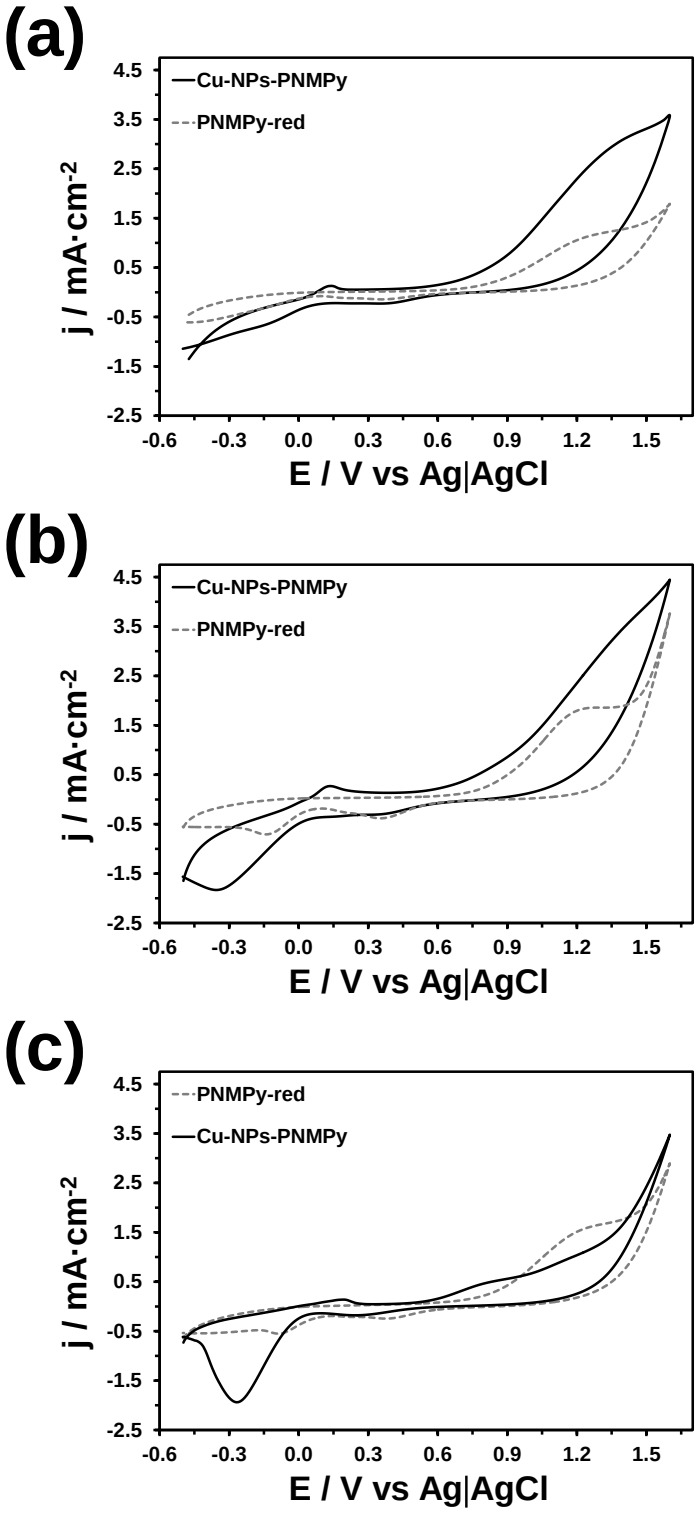
(a)
Cu-NPs-PNMPy
PNMPy-red
j / mA·cm-2
E / V vs Ag|AgCl
(b)
Cu-NPs-PNMPy
PNMPy-red
j / mA·cm-2
E / V vs Ag|AgCl
(c)
PNMPy-red
Cu-NPs-PNMPy
j / mA·cm-2
E / V vs Ag|AgCl

Figure 3

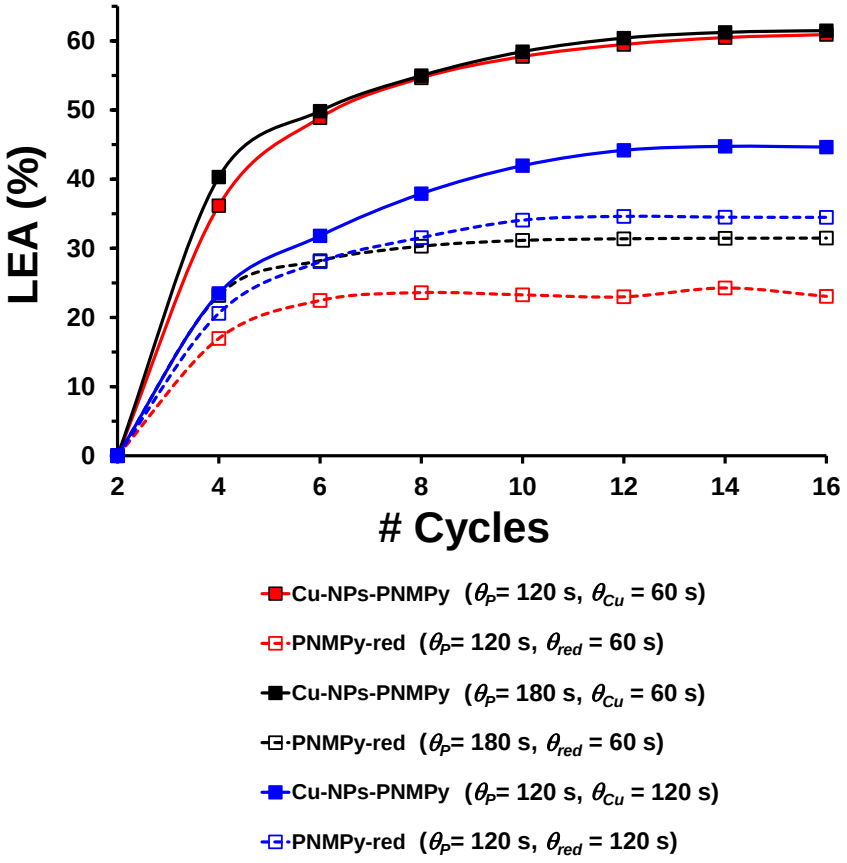
LEA (%)
60
50
40
30
20
10
0
2
4
6
8
10
12
14
16
Cycles
Cu-NPs-PNMPy (θ_P= 120 s, θ_{Cu} = 60 s)
PNMPy-red (θ_P= 120 s, θ_{red} = 60 s)
Cu-NPs-PNMPy (θ_P= 180 s, θ_{Cu} = 60 s)
PNMPy-red (θ_P= 180 s, θ_{red} = 60 s)
Cu-NPs-PNMPy (θ_P= 120 s, θ_{Cu} = 120 s)
PNMPy-red (θ_P= 120 s, θ_{red} = 120 s)

Figure 4

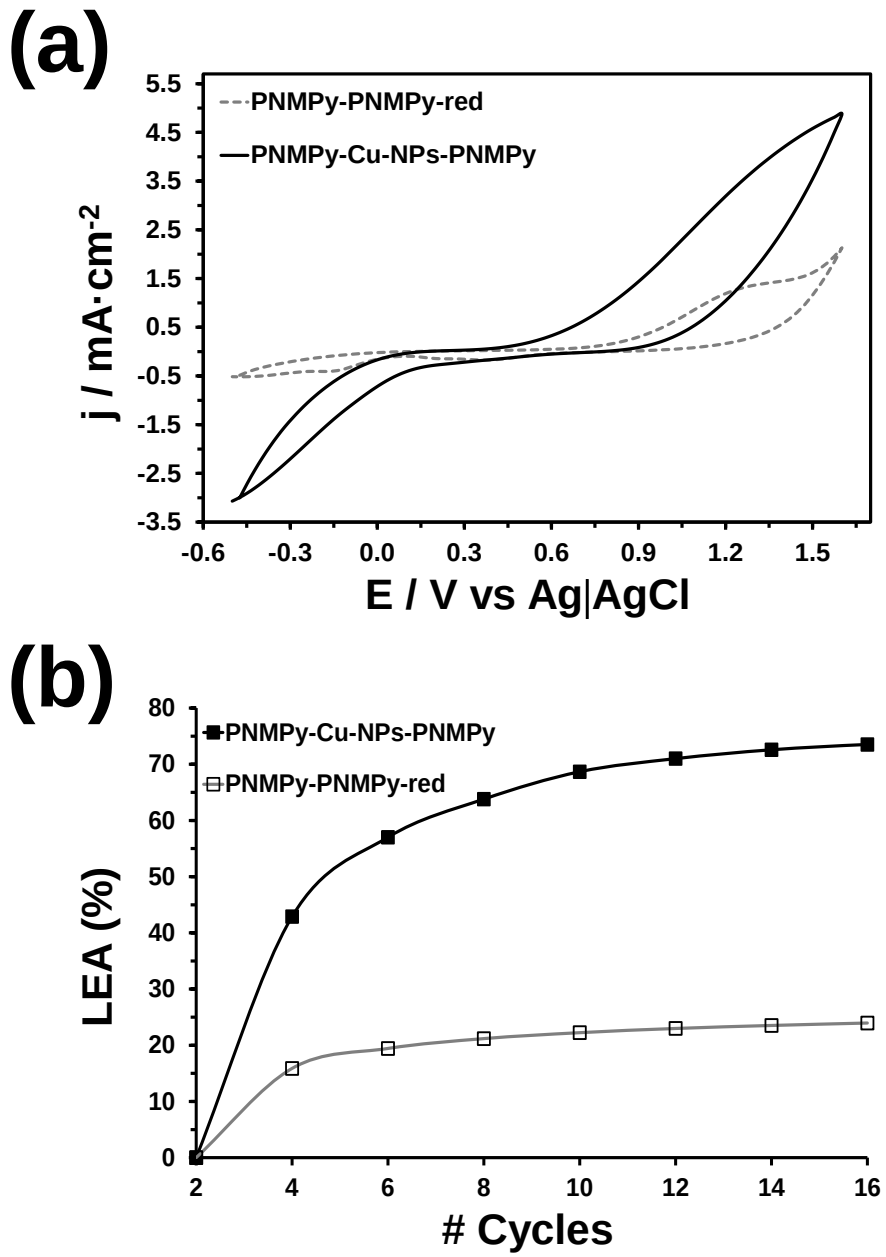
(a)
PNMPy-PNMPy-red
PNMPy-Cu-NPs-PNMPy
j / mA·cm-2
E / V vs Ag|AgCl
(b)
PNMPy-Cu-NPs-PNMPy
PNMPy-PNMPy-red
LEA (%)
Cycles

Figure 5